Letter

Refraction laws for two-dimensional plasmons

Dmitry A. Svintsov* and Georgy V. Alymov
Center for Photonics and 2D Materials, Moscow Institute of Physics and Technology, Dolgoprudny 141700, Russia

(Received 24 May 2023; accepted 15 September 2023; published 22 September 2023)

Despite numerous applications of two-dimensional (2D) plasmons for electromagnetic energy manipulation at the nanoscale, their quantitative refraction and reflection laws (analogs of Fresnel formulas in optics) have not yet been established. This fact can be traced to the strong nonlocality of equations governing the 2D plasmon propagation. Here, we tackle this difficulty by direct solution of the plasmon scattering problem with the Wiener-Hopf technique. We obtain the reflection and transmission coefficients for 2D plasmons at the discontinuity of 2D conductivity at arbitrary incidence angle, for both gated and nongated 2D systems. At a certain incidence angle, the absolute reflectivity has a pronounced dip, reaching zero for gated plasmons. The dip is associated with wave passage causing no dynamic charge accumulation at the boundary. For all incidence angles, the reflection has a nontrivial phase different from zero and π.

DOI: 10.1103/PhysRevB.108.L121410

Quantitative laws of wave reflection from a boundary between dissimilar media play a fundamental role in physics. In electrodynamics, such relations are known as Fresnel's formulas [1] and represent an indispensable tool for the design of any optical element, be it a cavity, polarizer, or antireflection coating. Similar laws can be found in the acoustics of gases, liquids, and solids [2]. In quantum mechanics, the problem of reflection and transmission at a potential step is a primary tool to demonstrate the wavelike nature of elementary particles.

Electromagnetically thin conductive media, be it two-dimensional (2D) materials, quantum wells, or inversion layers in semiconductors, support a special type of electromagnetic waves known as two-dimensional plasmons [3–5]. At realistic densities of charge carriers, they can be confined by $\sim 10^2$ times compared to the free-space electromagnetic wavelength in vacuum [6]. This fact motivates their application for compact light detectors [7–9] and sources [10,11], as well as for the observation of zero-point electromagnetic fluctuation phenomena at the macroscale [12].

Given the above motivation, it is surprising that quantitative Fresnel-type laws of 2D plasmon reflection have not been derived. The complexity of such derivation stems from the strong nonlocality of the dynamic equations governing the wave propagation. As a result of nonlocality, wavelike solutions break down at the interface of two conductive media. A conventional scheme of reflectance and transmittance derivation based on matching the field amplitudes at the interface [13] becomes invalid. A number of works dealt with approximate reflection laws for 2D plasmons using numerical techniques [14–17] and simulators [18], yet exact expressions for reflectance and transmittance have not been obtained.

Here, we resolve this complexity by a direct solution of the scattering integral equation in a piecewise-uniform 2D medium with the Wiener-Hopf technique. The latter was widely applied to the diffraction problems at semi-infinite objects (wedges [19], waveguide terminations [20], and others). It was used many years ago in the problem of surface wave reflection at the normal incidence between metals with dissimilar surface impedances [21] and, quite recently, to 2D plasmon scattering *at normal incidence* [22]. A problem of *inclined incidence* is more complicated due to the presence of two nontrivial field projections, wherein two coupled integral equations are formed [23]. The Wiener-Hopf method is generally inapplicable in these situations [24]. The latter complexity is resolved in the quasistatic (potential) approximation. Such approximation is successfully used to describe the spectrum of edge magnetoplasmons [25] and similar waves [26–28].

We obtain a full analytical solution for 2D plasmon reflection and transmission at the interface between 2D electron systems (2DES) with different conductivities at arbitrary incidence angle α. In addition to the total internal reflection, we find a certain angle α^* at which the reflection is minimized. The reflection falls completely to zero if the wave propagates in the presence of the ground plane (gated plasmon). This phenomenon may look similar to the Brewster effect in optics, but has a different origin. At this angle α^*, the incident and transmitted waves cause no accumulation of charge at the interface; hence, no physical reason for reflection appears. For nongated plasmons, the reflection coefficient has a nontrivial phase shift which becomes large in the case of gliding incidence.

We proceed to the solution of the scattering problem schematically shown in Fig. 1(a). The plasmon is incident from the left section, with conductivity σ_L, at the boundary with the right section, with conductivity σ_R, at angle α. It causes reflected (r) and transmitted (t) waves. All wave characteristics (potential φ, current density $\mathbf{j}$) are harmonically varying in time as $e^{-i\omega t}$; this time-dependent term will be skipped. The frequency dependence of conductivity $\sigma(\omega)$ can be arbitrary. The only requirement is that σ has a large positive imaginary part such that transverse-magnetic 2D plasmons are well defined.

*svintcov.da@mipt.ru

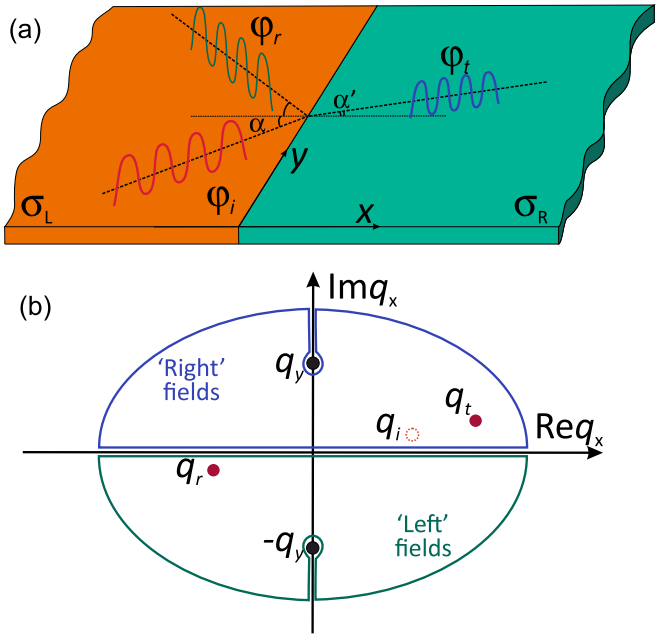

FIG. 1. (a) Schematic of the problem: A 2D plasmon (red) is incident from the left on the conductivity step from σ_L to σ_R, causing a reflected wave (green) and a transmitted wave (blue). Incidence angle is α; refraction angle is α'. (b) Analytic structure of the Fourier-transformed scattering equation. The dielectric functions $\varepsilon_{L/R}(q_x)$ have branch cuts starting at $\pm iq_y$ and running to $\pm i\infty$. They have simple zeros at wave vectors of the incident, transmitted, and reflected waves, $q_x = \{q_i,\ q_t,\ q_r\}$. The "incident" zero is compensated by the pole of the Fourier-transformed incident potential (shown with hollow circle).

The governing equation for electric potential $\Phi(r)$ in the 2D plane can be presented symbolically as

$$\Phi(r) = \mathcal{L}[\Phi], \tag{1}$$

where $\mathcal{L}[\cdot]$ is the integro-differential linear operator linking the potential created by charges in 2DES to the nonuniform field producing these charges,

$$\mathcal{L}[f] = \frac{1}{i\omega}\int d^2r' G(r-r')\nabla_{r'}[\sigma(r')\nabla_{r'}f(r')]. \tag{2}$$

Above, $G(r) = |r|^{-1} - |r^2 + 4d^2|^{-1/2}$ is the Green's function of the electrostatic problem, d is the distance to the screening plate (gate), and $\sigma(r)$ is the distribution of 2D conductivity, $\sigma(r) = \sigma_L\theta(-x) + \sigma_R\theta(x)$.

To solve the scattering problem, we split the full potential into the incident and scattered fields, $\Phi = \varphi_i + \varphi$. We choose the incident field as a semibounded plasma wave $\varphi_i(r) = \varphi_i \exp(iq_i x + iq_y y)\theta(-x)$. After such decomposition, the governing equation for scattered fields φ takes the form

$$\varphi(r) = \{\mathcal{L}[\varphi_i] - \varphi_i(r)\} + \mathcal{L}[\varphi]. \tag{3}$$

We recognize that the term in curly brackets is equivalent to the "external source" creating the scattered field. From now on, the solution of the scattering problem for 2D plasmons will not be much different from the solution of half-plane diffraction problems under external free-space illumination that have been extensively studied [19,29–31].

We apply two subsequent Fourier transforms to Eq. (3). The first one with respect to the y coordinate is trivial. The emerging wave vector q_y will be considered as an independent variable of the problem, the conserved y component of plasmon momentum. Further on, we split the scattered potential into the "left" and "right" functions, $\varphi_{q_y}(x) = \varphi_L(x)\theta(-x) + \varphi_R(x)\theta(x)$, and apply the second Fourier transform $F[\varphi](q_x) = \int_{-\infty}^{+\infty}\varphi(x)e^{-iq_x x}dx$ with respect to the x coordinate. This leads us to the fully Fourier-transformed scattering problem,

$$\varepsilon_L(q_x)[\varphi_i(q_x) + \varphi_L(q_x)] + \varepsilon_R(q_x)\varphi_R(q_x) = \frac{q_x}{\omega}G(q)[\sigma_R - \sigma_L]\varphi_0, \tag{4}$$

where we have introduced the effective 2D dielectric functions of the left and right media,

$$\varepsilon_\alpha(q_x) = 1 + \frac{i\sigma_\alpha}{\omega}q^2 G(q), \quad \alpha = \{L,\ R\}, \tag{5}$$

and the Fourier-transformed Green's function of the electrostatic problem, $G(q) = 2\pi q^{-1}(1 - e^{-2qd})$, $q = [q_x^2 + q_y^2]^{1/2}$. The term on the right-hand side containing the value of the real-space potential at the boundary, $\varphi_{q_y}(0) \equiv \varphi_0$, has emerged due to the discontinuous electric field.

The solution of (4) is based on the inspection of the analytic properties of the emerging functions in the plane of the complex q_x variable and is given in the Supplemental Material, Sec. I [32]. The main property is that two functions $F_+(q_x)$ and $F_-(q_x)$, being analytic in the upper and lower half-planes and identical in the stripe $|\operatorname{Im} q_x| < \delta$, should be equal to a polynomial of complex q_x. This polynomial degenerates to zero if we require finiteness of potentials at infinity. Such splitting of Eq. (4) is quite straightforward if we know the decomposition of dielectric function $\varepsilon_\alpha(q_x) = \varepsilon_\alpha^+(q_x)\varepsilon_\alpha^-(q_x)$ into the functions that are analytic and free of zeros in the upper (+) and lower (−) half-planes. In any case, it can be achieved with the general formula

$$\varepsilon_\alpha^\pm(q_x) = \exp\left\{\pm\frac{1}{2\pi i}\int_{-\infty}^{+\infty}\frac{\ln\varepsilon_\alpha(u)du}{u - q_x \pm i0^+}\right\}. \tag{6}$$

The direct numerical integration in Eq. (6) is complex due to the slow convergence at infinity and due to the presence of dielectric function zeros generating the singularities of $\ln\varepsilon$. Both difficulties can be successfully handled as described in the Supplemental Material, Sec. II [32].

The result of splitting for the scattering equation (4) reads

$$[M_+(q_x) - M_+(q_i)]\varphi_i(q_x) + M_+(q_x)\varphi_L(q_x) - i\frac{\varphi_0}{2}L_+(q_x) = -M_+(q_i)\varphi_i(q_x) - M_-(q_x)\varphi_R(q_x) + i\frac{\varphi_0}{2}L_-(q_x), \tag{7}$$

$$M_+(q_x) = \frac{\varepsilon_L^+(q_x)}{\varepsilon_R^+(q_x)}, \quad M_-(q_x) = \frac{\varepsilon_R^+(q_x)}{\varepsilon_-^+(q_x)}, \tag{8}$$

$$L_\pm(q_x) = \pm\frac{M_\pm(q_x)}{q_x \pm iq_y} \pm \frac{M_\pm(q_x) - M_\pm(\pm iq_y)}{q_x \mp iq_y} \mp \frac{M_\mp(\mp iq_y)}{q_x \pm iq_y}. \tag{9}$$

The left- and right-hand sides of such equation are now analytic in the upper and lower half-planes, respectively. They are identical in the stripe $|\operatorname{Im} q_x| < \operatorname{Im} q_i$, where $\operatorname{Im} q_i$ is the

decay constant of the incident wave (which can approach zero in the final result). Hence, both sides are identically zero, which yields the solution for the scattering problem in the Fourier space,

$$\varphi_L(q_x) = M_+^{-1}(q_x)\left\{i\frac{\varphi_0}{2}L_+(q_x) - [M_+(q_x) - M_+(q_i)]\varphi_i(q_x)\right\}, \tag{10}$$

$$\varphi_R(q_x) = M_-^{-1}(q_x)\left\{i\frac{\varphi_0}{2}L_-(q_x) - M_+(q_i)\varphi_i(q_x)\right\}. \tag{11}$$

A remaining problem is to link the real-space potential at $x = 0$, φ_0, to that in the incident wave, φ_i. This is achieved by evaluating the inverse transform $\varphi_L(0^-) = \pi^{-1}\lim_{x\to 0^-}\int_{-\infty}^{+\infty}\varphi_L(q_x)e^{iq_x x}dq_x$ and solving a simple self-consistency system. This leads to

$$\varphi_0 = 2\varphi_i\frac{M_+(q_i)}{M_+(iq_y) + M_-(-iq_y)}, \tag{12}$$

and completes the formal solution.

The real-space fields $\varphi_L(x)$ and $\varphi_R(x)$ are evaluated by inverse Fourier transforms of (10) and (11). The spatial structure of the fields becomes transparent if we close the integration path in the expressions for inverse Fourier transforms in the upper half plane (UHP) (for "right" fields) and in the lower half plane (LHP) (for "left" fields), as shown in Fig. 1(b). The contribution to $\varphi_{L/R}(x)$ from the integration path enclosing the branch cuts of the dielectric function emanating at $q_x = \pm iq_y$ yields the evanescent fields localized near the boundary. These fields decay at the distance $\Delta x \sim q_y^{-1}$ from the edge. It is the presence of evanescent fields which renders the plane-wave matching procedure for the derivation of the plasmons' refraction laws inapplicable. The contribution to $\varphi_{L/R}(x)$ from residues at the poles $q_x = q_r$ and $q_x = q_t$ yields the amplitudes or transmitted and reflected plasmons, respectively,

$$r = \frac{M_+(q_i)}{\partial M_+/\partial q_x|_{q_x=q_r}}\left\{\frac{1}{q_r - q_i} - \frac{q_r}{q_r^2 + q_y^2} - \frac{iq_y}{q_r^2 + q_y^2}\frac{M_+^2(iq_y) - 1}{M_+^2(iq_y) + 1}\right\}, \tag{13}$$

$$t = \frac{1}{\partial M_-/\partial q_x|_{q_x=q_t}}\left\{\frac{M_+(q_i)}{q_t - q_i} - M_+(q_t)\left[\frac{2q_t}{q_t^2 + q_y^2} - \frac{iq_y}{q_t^2 + q_y^2}\frac{M_-^2(-iq_y) - 1}{M_-^2(-iq_y) + 1}\right]\right\}. \tag{14}$$

Equations (13) and (14) represent the central result of this paper. To check its correctness, we note that for small separation between the gate and 2DES, $qd \ll 1$, the dielectric function $\varepsilon_\alpha^G(q_x)$ has a very simple analytic structure. Namely, $\varepsilon_\alpha^G(q_x) = 1 - (q_x^2 + q_y^2)/q_{p\alpha}^2$, where $q_{p\alpha}^2 = i\omega/4\pi d\sigma_\alpha$, $\alpha = \{L, R\}$, is the absolute value of the plasmon wave vector. The factorization of such dielectric function is immediately achieved,

$$\varepsilon_\alpha^G(q_x) = \frac{\sqrt{q_{p\alpha}^2 - q_y^2} - q_x}{q_{p\alpha}}\frac{\sqrt{q_{p\alpha}^2 - q_y^2} + q_x}{q_{p\alpha}}. \tag{15}$$

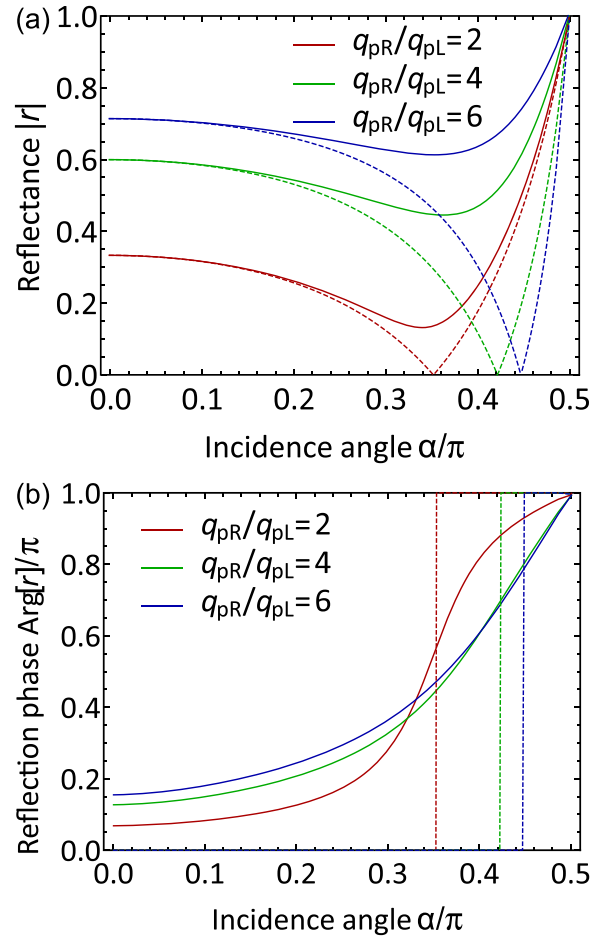

FIG. 2. Computed reflectances $|r|$ and reflection phases arg$r$ for a two-dimensional plasmon incident from the medium with high conductivity to the medium with low conductivity ($\mathrm{Im}\sigma_L > \mathrm{Im}\sigma_R$, $q_{pL} < q_{pR}$). Solid lines represent the result for nongated plasmons, while dashed lines correspond to gated 2D plasmons.

Introducing (15) into (13), we get very simple refraction laws for gated plasmons,

$$r^G = \frac{q_{pL}^2\sqrt{q_{pR}^2 - q_y^2} - q_{pR}^2\sqrt{q_{pL}^2 - q_y^2}}{q_{pL}^2\sqrt{q_{pR}^2 - q_y^2} + q_{pR}^2\sqrt{q_{pL}^2 - q_y^2}}. \tag{16}$$

The same result is obtained in a simpler fashion by matching the potential and current across the boundary. The matching approach is correct for strong gate screening, where electrostatics become local. Hence, the identity of the Wiener-Hopf result with the wave matching result in the gated case serves as a check for this complex method. On the other hand, the matching approach does not apply to the nongated plasmons, and we have to deal with full Wiener-Hopf expressions for reflection (13) and transmission (14).

The computed reflection coefficient, according to Eq. (13), is shown in Figs. 2 and 3, for both the absolute value and phase. Expressing the parameters of the left and right 2DES sections through the respective absolute values of plasmon wave vector q_{pL} and q_{pR}, we can present the result in unified fashion for nongated and gated plasmons. These are shown

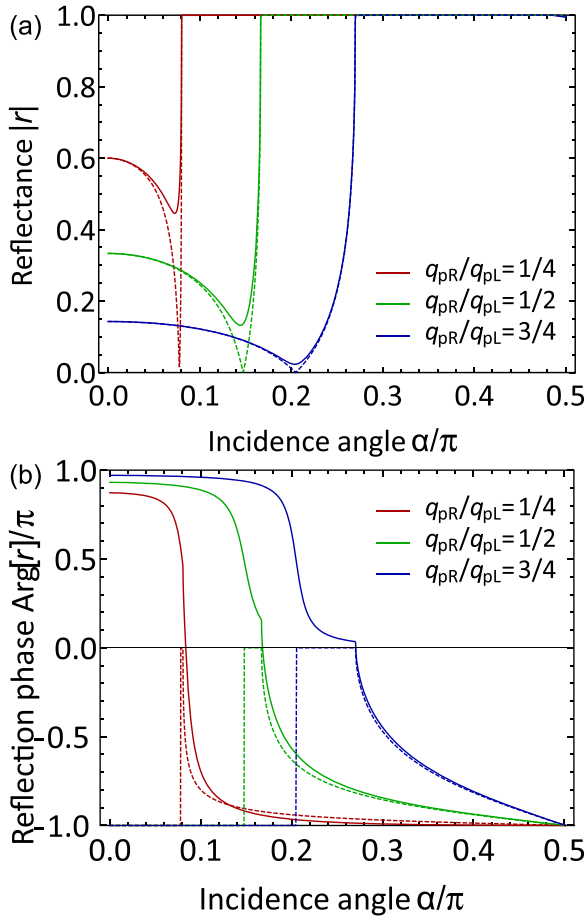

FIG. 3. Computed reflectances $|r|$ and reflection phases $\arg r$ for a two-dimensional plasmon incident from the medium with low conductivity to the medium with high conductivity ($\mathrm{Im}\sigma_L < \mathrm{Im}\sigma_R$, $q_{pL} > q_{pR}$). Solid lines represent the result for nongated plasmons, while dashed lines correspond to gated 2D plasmons.

with solid and dashed lines, respectively. It is possible to show that absolute reflectance falls to zero for gated plasmons at the incidence angle α^*, satisfying the Brewster-type condition,

$$\tan\alpha^* = \frac{q_{pR}}{q_{pL}}. \tag{17}$$

For nongated plasmons, the reflectance (13) has a dip not reaching zero, but becoming more pronounced for smaller "contrast" of left and right sections. A similar dip was observed in electromagnetic simulations [18].

It is tempting to associate a dip in transmission with the Brewster effect in conventional optics. In that case, the reflected wave vector should be codirectional with the light-induced dipole moment in the medium no. 2, but the dipole intensity in such direction turns to zero. Such explanation does not apply in the case of 2D plasmons, which have an electric vector parallel to the propagation direction. The dipole emission intensity is thus always nonzero in the direction of the 2D plasmon reflection. Finally, the concept of canonical dipole radiation does not apply to 2D plasmons treated in the nonretarded approximation, $c \to \infty$.

A careful analysis shows that the induced charges at the boundary of two 2DES sections do not appear at all at the nonreflection angle α^*. More precisely, the magnitudes of surface currents $\mathbf{j}$ in the incident and transmitted wave are fine tuned to cause no linear charge accumulation at the boundary. As a result, no physical stimulus appears for the reflection. To prove this viewpoint, we rewrite the no-reflection conduction (17) via conductivity and wave vector

$$\sigma_L q_i = \sigma_R q_t. \tag{18}$$

This is precisely the condition of current continuity $j_x = -\sigma(x)\varphi'(x)$ between the incident and transmitted waves. Invoking the charge continuity equation, $-i\omega\rho + (\nabla\cdot\mathbf{j}) = 0$, we observe that continuity of the current implies the absence of line charge.

Interestingly, the reflection dip for nongated plasmons never reaches zero. This fact is linked to the emergence of evanescent fields near the interface. As a result, some charge accumulation in the boundary layer should appear for nongated plasmons, even despite the fulfillment of the current matching condition (18). The latter condition applies only to the plane-wave part of the solution, and does not include the evanescent fields.

The second important property of nongated plasmon reflection, illustrated in Fig. 2(b), is the nontrivial reflection phase shift. It is different from zero and π, and grows monotonically with increasing the angle of incidence. The case of gated plasmons, shown in the same figure with dashed lines, demonstrates a simpler behavior. The phase shift changes here stepwise between zero and π at the nonreflection angle α^*. The latter situation is analogous to the reflection of p-polarized waves near the Brewster angle, though the origin of nonreflectance here is completely different.

The minimization of reflection for nongated plasmons, and its full absence for gated plasmons, also persists for incidence from the medium with low conductivity to the medium with high conductivity. As illustrated in Fig. 3, plotted for this case, the reflectance dip occurs at angles slightly below the angle of total internal reflection, α_{tir}. The variation of both the amplitude and phase of reflection is remarkably abrupt between α^* and α_{tir}. These strong variations would result in pronounced Goos-Hanchen shifts for the reflected waves [33]. In our particular 2D setup, Goos-Hanchen shift can be interpreted as the excitation of leaky interedge plasmons [34]. From a practical viewpoint, abrupt phase variations can be used for sensing applications, wherein the identified object modifies the properties of 2D conductivity [35].

The obtained solution of the scattering problem is generic and applies to arbitrary 2DES once their complex conductivity σ at the incident wave frequency ω is known. The functional dependence $\sigma(\omega)$ is not limited to the Drude model and, if necessary, may be invoked from quantum models [36] or from experiment [37,38]. The inclusion of nonlocal conduction effects is more challenging, yet is formally possible within the hydrodynamic approach to electron transport [39]. Within such an approach, it is possible to study the effects of electron diffusion, viscosity [39], and dc bias current [40] on the plasmon reflection at the boundary. The effect of dc current is particularly interesting as it can lead to amplified wave reflection [41]. Such extensions require considerable analytical effort. Yet, we anticipate that the resulting expressions for r and t would be expressed via two split functions, $\varepsilon^{\pm}(q_x)$, and

the complexity of their numerical evaluation would amount to a single one-dimensional integration.

Once the reflection coefficients of 2D plasmons at a single boundary are known, more complex 2D optical elements can be computed and designed. As an example, the reflection and transmission by a stripe in 2DES with conductivity contrast can be computed using the quasi-optical approach. Such stripe can be considered as a 2D analog of a Fabry-Perot cavity (notch filter for 2D waves) and also as a waveguide for 2D plasmons. The spectrum of plasmons in such a waveguide $q_y(\omega)$ can be inferred from the poles of the transmission amplitude. We can foresee that guided mode spectra for 2D plasmons would differ from the analogous spectra for 3D electromagnetic waves due to the nontrivial reflection phase shift. Applications of 2D plasmonic waveguides can be suggested for ultracompact on-chip signal transmitters [42], while 2D cavities formed by stripes with alternating doping are already applied for ultralong-wavelength radiation detection, emission, and modulation [11,43,44]. Further extensions of our computational method can be applied to cavities formed by the gating of 2DES [45–47].

The obtained reflection and transmission coefficients can also be applied for the design of 2D optical structures with curved boundaries, once the curvature radius exceeds the wavelength. A curved boundary in 2DES can act as a lens for 2D plasmons. Again, the focal distance of such a lens would have a nontrivial dependence on the refractive index due to the plasmon phase shift at a single boundary.

This work was supported by the Russian Science Foundation (Grant No. 21-72-10163).

[1] A.-J. Fresnel, On the calculation of the tints that polarization develops in crystalline plates, Ann. Chim. Phys. **17**, 102 (1821).

[2] L. D. Landau and E. M. Lifshitz, *Fluid Mechanics*, Course of Theoretical Physics Vol. 6 (Elsevier, Amsterdam, 2013).

[3] F. Stern, Polarizability of a Two-Dimensional Electron Gas, Phys. Rev. Lett. **18**, 546 (1967).

[4] S. J. Allen, D. C. Tsui, and R. A. Logan, Observation of the Two-Dimensional Plasmon in Silicon Inversion Layers, Phys. Rev. Lett. **38**, 980 (1977).

[5] A. V. Chaplik, Possible crystallization of charge carriers in low-density inversion layers, Zh. Eksp. Teor. Fiz. **62**, 746 (1972) [Sov. Phys. JETP **35**, 395 (1972)].

[6] D. A. Iranzo, S. Nanot, E. J. C. Dias, I. Epstein, C. Peng, D. K. Efetov, M. B. Lundeberg, R. Parret, J. Osmond, J. Y. Hong, J. Kong, D. R. Englund, N. M. R. Peres, and F. H. L. Koppens, Probing the ultimate plasmon confinement limits with a van der Waals heterostructure, Science **360**, 291 (2018).

[7] V. M. Muravev, A. A. Fortunatov, A. A. Dremin, and I. V. Kukushkin, Plasmonic interferometer for spectroscopy of microwave radiation, JETP Lett. **103**, 380 (2016).

[8] W. Knap, Y. Deng, S. Rumyantsev, J.-Q. Lü, M. S. Shur, C. A. Saylor, and L. C. Brunel, Resonant detection of subterahertz radiation by plasma waves in a submicron field-effect transistor, Appl. Phys. Lett. **80**, 3433 (2002).

[9] D. A. Bandurin, D. Svintsov, I. Gayduchenko, S. G. Xu, A. Principi, M. Moskotin, I. Tretyakov, D. Yagodkin, S. Zhukov, T. Taniguchi, K. Watanabe, I. V. Grigorieva, M. Polini, G. N. Goltsman, A. K. Geim, and G. Fedorov, Resonant terahertz detection using graphene plasmons, Nat. Commun. **9**, 5392 (2018).

[10] A. El Fatimy, N. Dyakonova, Y. Meziani, T. Otsuji, W. Knap, S. Vandenbrouk, K. Madjour, D. Théron, C. Gaquiere, M. A. Poisson, S. Delage, P. Prystawko, and C. Skierbiszewski, AlGaN/GaN high electron mobility transistors as a voltage-tunable room temperature terahertz sources, J. Appl. Phys. **107**, 024504 (2010).

[11] S. Boubanga-Tombet, W. Knap, D. Yadav, A. Satou, D. B. But, V. V. Popov, I. V. Gorbenko, V. Kachorovskii, and T. Otsuji, Room-Temperature Amplification of Terahertz Radiation by Grating-Gate Graphene Structures, Phys. Rev. X **10**, 031004 (2020).

[12] E. Orgiu, J. George, J. A. Hutchison, E. Devaux, J. F. Dayen, B. Doudin, F. Stellacci, C. Genet, J. Schachenmayer, C. Genes, G. Pupillo, P. Samorì, and T. W. Ebbesen, Conductivity in organic semiconductors hybridized with the vacuum field, Nat. Mater. **14**, 1123 (2015).

[13] S. Inampudi and H. Mosallaei, Fresnel refraction and diffraction of surface plasmon polaritons in two-dimensional conducting sheets, ACS Omega **1**, 843 (2016).

[14] B.-Y. Jiang, E. J. Mele, and M. M. Fogler, Theory of plasmon reflection by a 1D junction, Opt. Express **26**, 17209 (2018).

[15] S. Siaber, S. Zonetti, and O. Sydoruk, Junctions between two-dimensional plasmonic waveguides in the presence of retardation, J. Opt. **21**, 105002 (2019).

[16] V. Semenenko, M. Liu, and V. Perebeinos, Scattering of Quasistatic Plasmons From One-Dimensional Junctions of Graphene: Transfer Matrices, Fresnel Relations, and Nonlocality, Phys. Rev. Appl. **14**, 024049 (2020).

[17] A. J. Chaves, B. Amorim, Y. V. Bludov, P. A. D. Goncalves, and N. M. R. Peres, Scattering of graphene plasmons at abrupt interfaces: An analytic and numeric study, Phys. Rev. B **97**, 035434 (2018).

[18] S. Farajollahi, B. Rejaei, and A. Khavasi, Reflection and transmission of obliquely incident graphene plasmons by discontinuities in surface conductivity: Observation of the Brewster-like effect, J. Opt. **18**, 075005 (2016).

[19] T. B. A. Senior, Diffraction by a semi-infinite metallic sheet, Proc. R. Soc. London A **213**, 436 (1952).

[20] H. M. Nussenzveig, Solution of a diffraction problem - Solution of a diffraction problem. I The wide double wedge, Philos. Trans. R. Soc. London. Ser. A, Math. Phys. Sci. **252**, 1 (1959).

[21] A. Kay, Scattering of a surface wave by a discontinuity in reactance, IRE Transact. Antennas Propagat. **7**, 22 (1959).

[22] B. Rejaei and A. Khavasi, Scattering of surface plasmons on graphene by a discontinuity in surface conductivity, J. Opt. **17**, 75002 (2015).

[23] V. G. Daniele, R. Zich *et al.*, *The Wiener-Hopf Method in Electromagnetics* (SciTech Publishing, Edison, NJ, 2014).

[24] A. A. Zabolotnykh and V. Volkov, Edge plasmon polaritons on a half-plane, JETP Lett. **104**, 411 (2016).

[25] V. A. Volkov and S. A. Mikhailov, Edge magnetoplasmons: Low frequency weakly damped excitations in inhomogeneous two-dimensional electron systems, Zh. Eksp. Teor. Fiz. **94**, 217 (1988) [Sov. Phys. JETP **67**, 1639 (1988)].

[26] A. Principi, M. I. Katsnelson, and G. Vignale, Edge Plasmons in Two-Component Electron Liquids in the Presence of Pseudomagnetic Fields, Phys. Rev. Lett. **117**, 196803 (2016).

[27] A. S. Petrov, Plasmonic excitation for a tunable transmitter without magnetic field immune to backscattering, Phys. Rev. B **104**, L241407 (2021).

[28] A. A. Sokolik, O. V. Kotov, and Y. E. Lozovik, Plasmonic modes at inclined edges of anisotropic two-dimensional materials, Phys. Rev. B **103**, 155402 (2021).

[29] Z. Lei, F. Xiu-Li, and Y. Jun-Zhong, Excitation of propagating plasmons in semi-infinite graphene layer by free space photons, Commun. Theor. Phys. **61**, 751 (2014).

[30] D. Margetis, M. Maier, and M. Luskin, On the wiener-hopf method for surface plasmons: Diffraction from semiinfinite metamaterial sheet, Stud. Appl. Math. **139**, 599 (2017).

[31] E. Nikulin, D. Mylnikov, D. Bandurin, and D. Svintsov, Edge diffraction, plasmon launching, and universal absorption enhancement in two-dimensional junctions, Phys. Rev. B **103**, 085306 (2021).

[32] See Supplemental Material at http://link.aps.org/supplemental/10.1103/PhysRevB.108.L121410 for details of Wiener-Hopf factorization of the scattering problem (Sec. I) and evaluation of split functions for effective 2D dielectric permeability $\varepsilon(q)$ (Sec. II).

[33] K. Artmann, Berechnung der seitenversetzung des totalreflektierten strahles, Annal. Phys. (Leipzig) **437**, 87 (1948).

[34] S. A. Mikhailov and V. A. Volkov, Inter-edge magnetoplasmons in inhomogeneous two-dimensional electron systems, J. Phys.: Condens. Matter **4**, 6523 (1992).

[35] D. Rodrigo, O. Limaj, D. Janner, D. Etezadi, F. J. G. de Abajo, V. Pruneri, and H. Altug, Mid-infrared plasmonic biosensing with graphene, Science **349**, 165 (2015).

[36] L. A. Falkovsky and S. S. Pershoguba, Optical far-infrared properties of a graphene monolayer and multilayer, Phys. Rev. B **76**, 153410 (2007).

[37] G. A. Ermolaev, K. V. Voronin, M. K. Tatmyshevskiy, A. B. Mazitov, A. S. Slavich, D. I. Yakubovsky, A. P. Tselin, M. S. Mironov, R. I. Romanov, A. M. Markeev, I. A. Kruglov, S. M. Novikov, A. A. Vyshnevyy, A. V. Arsenin, and V. S. Volkov, Broadband optical properties of atomically thin PtS_2 and $PtSe_2$, Nanomaterials **11**, 3269 (2021).

[38] C. Cervetti, E. Heintze, B. Gorshunov, E. Zhukova, S. Lobanov, A. Hoyer, M. Burghard, K. Kern, M. Dressel, and L. Bogani, Sub-terahertz frequency-domain spectroscopy reveals single-grain mobility and scatter influence of large-area graphene, Adv. Mater. **27**, 2635 (2015).

[39] R. Cohen and M. Goldstein, Hall and dissipative viscosity effects on edge magnetoplasmons, Phys. Rev. B **98**, 235103 (2018).

[40] M. Dyakonov and M. Shur, Shallow Water Analogy for a Ballistic Field Effect Transistor: New Mechanism of Plasma Wave Generation by dc Current, Phys. Rev. Lett. **71**, 2465 (1993).

[41] S. Zonetti, S. Siaber, J. E. Cunningham, and O. Sydoruk, Scattering-induced amplification of two-dimensional plasmons: Electromagnetic modeling, J. Appl. Phys. **129**, 223103 (2021).

[42] J. T. Kim and S.-Y. Choi, Graphene-based plasmonic waveguides for photonic integrated circuits, Opt. Express **19**, 24557 (2011).

[43] A. Shuvaev, K. R. Dzhikirba, A. S. Astrakhantseva, P. A. Gusikhin, I. V. Kukushkin, and V. M. Muravev, Plasmonic metasurface created by a grating of two-dimensional electron strips on a substrate, Phys. Rev. B **106**, L161411 (2022).

[44] G. C. Dyer, G. R. Aizin, S. James Allen, A. D. Grine, D. Bethke, J. L. Reno, and E. A. Shaner, Induced transparency by coupling of Tamm and defect states in tunable terahertz plasmonic crystals, Nat. Photon. **7**, 925 (2013).

[45] O. Sydoruk, K. Choonee, and G. C. Dyer, Transmission and reflection of terahertz plasmons in two-dimensional plasmonic devices, IEEE Trans. Terahertz Sci. Technol. **5**, 486 (2015).

[46] A. S. Petrov, D. Svintsov, M. Rudenko, V. Ryzhii, and M. S. Shur, Plasma instability of 2D electrons in a field effect transistor with a partly gated channel, Intl. J. High Speed Electron. Syst. **25**, 1640015 (2016).

[47] G. R. Aizin and G. C. Dyer, Transmission line theory of collective plasma excitations in periodic two-dimensional electron systems: Finite plasmonic crystals and Tamm states, Phys. Rev. B **86**, 235316 (2012).